Journal of Sulfur Chemistry
Publication details, including instructions for authors and subscription information:
http://www.informaworld.com/smpp/title~content=t713926081

Synthesis, photophysical, and electrochemical properties of the sulfur analogs of the new 4,4'-pyrylogen electron transfer sensitizers

Edward L. Clennan[a]; Ajaya Kumar Sankara Warrier[a]; Navamoney Arulsamy[a]
[a] Department of Chemistry, University of Wyoming, Laramie, WY, USA

To cite this Article Clennan, Edward L. , Kumar Sankara Warrier, Ajaya and Arulsamy, Navamoney(2009) 'Synthesis, photophysical, and electrochemical properties of the sulfur analogs of the new 4,4'-pyrylogen electron transfer sensitizers', Journal of Sulfur Chemistry, 30: 3, 212 — 224
To link to this Article: DOI: 10.1080/17415990902774228
URL: http://dx.doi.org/10.1080/17415990902774228

Journal of Sulfur Chemistry
Vol. 30, Nos. 3–4, June–August 2009, 212–224

Taylor & Francis
Taylor & Francis Group

Synthesis, photophysical, and electrochemical properties of the sulfur analogs of the new 4,4′-pyrylogen electron transfer sensitizers

Edward L. Clennan*, Ajaya Kumar Sankara Warrier and Navamoney Arulsamy

Department of Chemistry, University of Wyoming, 1000 East University Avenue, Laramie, WY 82071, USA

(*Received 27 December 2008; final version received 24 January 2009*)

This paper is dedicated to Professor Juzo Nakayama on the occasion of his 65th birthday and retirement.

A series of 2,6-diaryl-4,4′-thiapyrylogen bis-tetrafluoroborates have been prepared from 1,5-diketone precursors by treatment with H_2S and $BF_3 \bullet Et_2O$. The photophysical and electrochemical properties of these new sensitizers and 2,6-diphenyl-4,4′-pyrylogen bis-tetrafluoroborate have been compared and observed trends have been rationalized using B3LYP/6-31G(d) calculations.

Keywords: pyrylium; electron transfer; pyrylogen; sensitizer; cyclic voltammetry

1. Introduction

Pyrylium salts, $\mathbf{1}^+$, have been known for over 100 years (*1*). They are present as natural products in anthocyanin pigments, which are responsible for the blue or red color of several flowers and fruits (*2*). They have been explored as light-activated sensitizers in photodynamic therapy of cancer (*3,4*). Their fluorescent properties have also resulted in their use as laser dyes (*5*). Early fascination with these materials revolved around their benzenoid-like sextet of electrons which

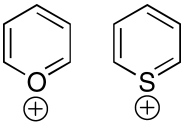

$\mathbf{1}^+$ $\mathbf{2}^+$

*Corresponding author. Email: clennane@uwyo.edu

ISSN 1741-5993 print/ISSN 1741-6000 online

DOI: 10.1080/17415990902774228
http://www.informaworld.com

impart aromatic character to these cationic heterocycles (*6*). In recent years, interest has focused on their use as electron-deficient photochemical sensitizers in electron transfer reactions (*7*).

Thiapyrylium salts, $\mathbf{2}^{+}$, were first reported nearly 50 years after the discovery of their oxygen homologs and were obtained from the reactions of pyrylium salts with sodium sulfide (*8*). The thiapyrylium salts are more stable than the pyrylium salts under a variety of reaction conditions (*1*). Nevertheless, they have not been found in nature (*1*) and have received far less attention than the pyrylium cations.

In 2008, we introduced a new class of electron transfer sensitizer for which we coined the name *pyrylogens*, $\mathbf{3}^{2+}$, in recognition of the fact that they are hybrids of pyrylium cations and viologens (*9*). These compounds, which have superior optical properties in comparison to viologens (*10*), were introduced in order to extend the concept of charge-shift reactions (*11*) from cationic to dicationic sensitizers. A charge-shift electron transfer from an electron-rich neutral substrate to the pyrylogen dication generates mutually repulsive radical cations whose diffusive separation competes with energy-wasting return electron transfer, thereby increasing the quantum yield of product formation.

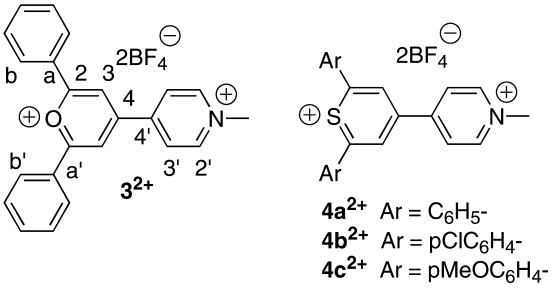

In this paper, we report the first synthesis of a series of thiapyrylogen salts, $\mathbf{4a–c}^{2+}$, their electrochemical, and their photophysical characterizations. We anticipate, in analogy to thiapyrylium cations (*5*,*12*), that the presence of the sulfur will enhance their intersystem crossings to the triplet excited states. Charge-shift reactions of the triplet excited states will generate triplet radical cation/radical cation pairs in which return electron transfer is spin forbidden. Consequently, we anticipate that these new sensitizers will further enhance the quantum yields of electron transfer reactions.

2. Results and discussion

2.1. *Synthesis and structural characterization*

Pyrylogens $\mathbf{4a\text{-}c}^{2+} \bullet \mathbf{2BF_4^-}$ were synthesized as shown in Scheme 1. Condensation of a phenone and pyridine-4-carbaldehyde generates an α,β-unsaturated ketone, which reacts via Michael addition with a second equivalent of phenone enolate to give a 1,5-diketone. Alkylation of pyridine nitrogen with trimethyloxonium tetrafluoroborate generates the pyridinium precursor for the formation of thiapyrylogen. Thiapyrylogens were generated, in the absence of any externally added hydride acceptor, using H_2S as the sulfur transfer agent. This reaction, which has been extensively used to generate thiapyrylium salts, has been suggested to occur via condensation to form a 4H-thiapyran intermediate (*1*). It was further suggested that this intermediate subsequently disproportionates to form the thiapyrylium salt, the dihydrothiapyran and eventually the tetrahydrothiapyran byproducts. However, the formation of $\mathbf{4b}^{2+} \bullet \mathbf{2BF_4^-}$ in 79% yield (see Experimental

section) is inconsistent with this disproportionation mechanism, which can theoretically produce a maximum yield of 67%. Consequently, aromatization via loss of hydride from the dihydrothiapyrylogen intermediate could also be occurring either during the recrystallization from acetic acid and acetonitrile, upon treatment with $BF_3 \bullet Et_2O$, or by oxidation with molecular oxygen that was not excluded during the reaction or subsequent recrystallization. Additional studies to explore the mechanistic details were not conducted.

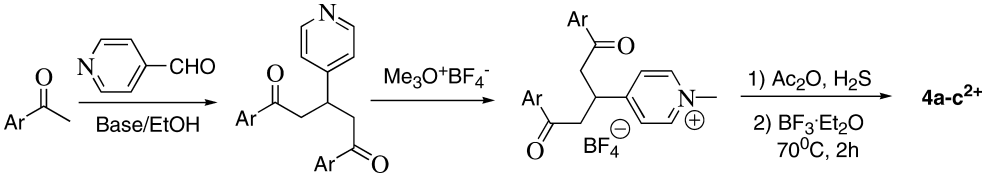

Scheme 1.

The ^{13}C and ^{1}H NMR chemical shifts of $\mathbf{4a–c}^{2+}$ were readily assigned by comparison to *N*-methyl-2,6-diphenyl-4, 4′-pyrylogen, $\mathbf{3}^{2+}$ (*9*). The C_2 carbon chemical shifts in $\mathbf{4a}^{2+}$ (173.9 ppm) and in $\mathbf{3}^{2+}$ (174.0 ppm) are remarkably similar. On the other hand, significantly different ^{13}C chemical shifts at C_3 and C_4 and ^{1}H chemical shift at H_3 were observed. H_3 in $\mathbf{4a}^{2+}$ at 9.02 ppm is deshielded by 0.2 ppm in comparison to H_3 in $\mathbf{3}^{2+}$. The larger downfield chemical shifts at the "meta" positions in thiapyrylium in comparison to pyrylium cations have been previously observed (*13*) and attributed to the participation of 3d orbitals on sulfur that allow contribution from resonance structures **10** and **11**, as shown in Scheme 2. The significant downfield shift of C_3 in $\mathbf{4a}^{2+}$ (128.2 ppm) in comparison to $\mathbf{3}^{2+}$ (119.0 ppm) is also consistent with contributions of resonance structures **10** and **11** that place positive charge on C_3. In contrast, the ∼5 ppm upfield shift of C_4 in $\mathbf{4a}^{2+}$ in comparison to $\mathbf{3}^{2+}$ is that anticipated based on the greater electronegativity of oxygen in comparison to sulfur.

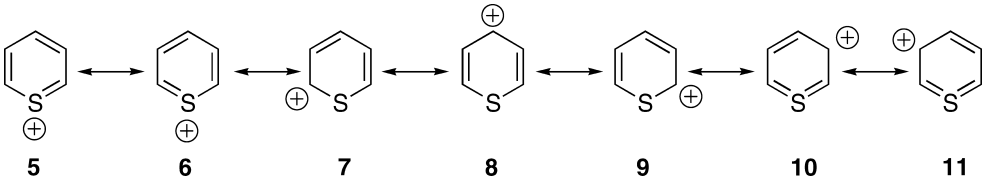

Scheme 2.

Unequivocal proof of structure was obtained by X-ray diffraction of $\mathbf{4a}^{2+} \bullet \mathbf{2BF_4^-}$, as shown by the four perspectives of the crystal structure depicted in Figure 1. Characteristic structural features include a significant deviation from planarity, as indicated by an inter-ring dihedral angle (>344′3′) of 46.41° and reasonably short S–C bond lengths of 1.702 and 1.705 Å, indicative of the double-bond character. The inter-ring carbon–carbon bond length (C_4–$C_{4'}$) is 1.493 Å, well within the range expected for an sp^2–sp^2 single bond. The two BF_4^- counterions are far more closely associated with the pyridinium (nitrogen–boron distances 3.952 and 4.085 Å) than with the thiapyrylium ring (sulfur–boron distances 6.816 and 9.659 Å).

We have not obtained X-ray crystal structures for $\mathbf{4b}^{2+}$ or $\mathbf{4c}^{2+}$ but have instead used the B3LYP/6-31G(d) computational method to explore their structures (*14*). The veracity of this method to give accurate structural data is readily demonstrated by comparison of the crystal structure of $\mathbf{4a}^{2+}$ to its B3LYP/6-31G(d) geometry, as shown in Table 1. A comparison of the computed structures reveals only minor effects of the substituents on the thiapyrylogen core geometry

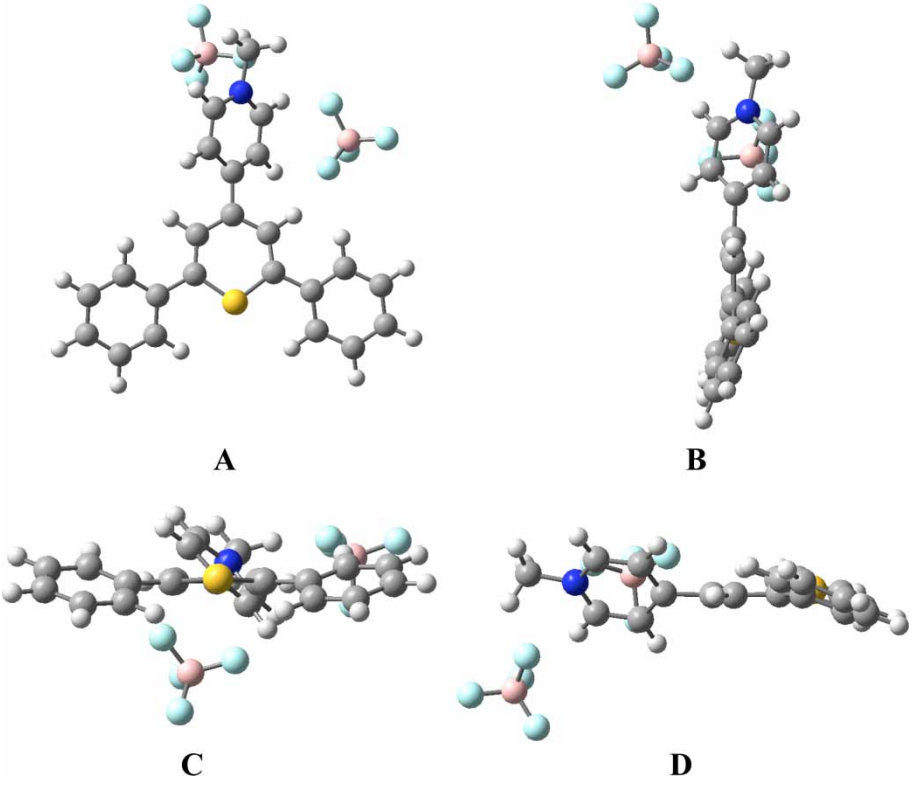

Figure 1. Four perspectives of the X-ray Structure of $\mathbf{4a}^{2+}$.

(Table 1). However, replacement of oxygen in pyrylogen $\mathbf{3}^{2+}$ with sulfur to give thiapyrylogens $\mathbf{4a–c}^{2+}$ leads to a significant decrease in the angle <216, which was also experimentally detected in the X-ray structure (Table 1).

Table 1. A comparison of X-ray and B3LYP/6-31G(d) structures for $\mathbf{4a–c}^{2+}$.[†‡]

	$\mathbf{3}^{2+}$	$\mathbf{4a}^{2+}$	$\mathbf{4a}^{2+}$(X-ray)	$\mathbf{4b}^{2+}$[§]	$\mathbf{4c}^{2+}$
d_{12}(Å)	1.354	1.739	1.702	1.742	1.751
d_{16}(Å)	1.354	1.738	1.705	1.742	1.751
$d_{44'}$(Å)	1.487	1.491	1.493	1.490	1.487
$d_{1'2'}$(Å)	1.355	1.355	1.343	1.355	1.355
$d_{1'6'}$(Å)	1.354	1.353	1.342	1.353	1.354
d_{2a}(Å)	1.445	1.460	1.479	1.457	1.447
$d_{6a'}$(Å)	1.445	1.460	1.470	1.457	1.447
>216	124.84°	105.87°	105.46°	105.88°	106.11°
>2′1′6″	120.25°	120.20°	121.12°	120.18°	120.07°
>344′3′	41.48°	43.32°	46.41°	43.18°	41.73°
>12ab	15.78°	31.50°	27.90°	29.51°	25.67°
>16a′b′	15.36°	32.09°	25.80°	30.08°	25.81°
3′2′NCH$_3$	178.18°	178.72°	174.25°	178.72°	178.48°

Notes: [†]ZPE corrected energies; $\mathbf{3}^{2+}$ – 1017.33267349 Hartrees; $\mathbf{4a}^{2+}$ – 1339.938753 Hartrees; $\mathbf{4b}^{2+}$ – 2259.140584 Hartrees; $\mathbf{4c}^{2+}$ – 1568.942214 Hartrees. [‡]See the structure of $\mathbf{3}^{2+}$ for labeling scheme of structures. [§]ii-isomer in which both methoxy methyl groups are pointing in towards pyrylium oxygen.

2.2. *Photophysical characterization*

The UV-visible spectra of **4a–c**$^{2+}$ are compared with those of **3**$^{2+}$ and 2,4,6-triphenylpyrylium tetrafluoroborate, **TPP**$^{+}$, in Figure 2. All of the pyrylogens absorb at longer wavelength than **TPP**$^{+}$. The pyrylogens are characterized by two large intensity bands and a low intensity band between these two absorbances that is barely visible in **4a**$^{2+}$ and **4b**$^{2+}$, is more prominent in **3**$^{2+}$, and appears as a shoulder on the low-energy absorbance in **4c**$^{2+}$. Time-dependent density functional calculations (TD-DFT) (*15*) suggest that in each case the lowest energy transition responsible for the long wavelength band is the HOMO to LUMO transition (inset in Figure 2). Indeed, these calculations suggest that the four lowest energy transitions with substantial oscillator strength (HOMO $\rightarrow$ LUMO; HOMO $-$ 3 $\rightarrow$ LUMO; HOMO $\rightarrow$ LUMO + 1; and HOMO $\rightarrow$ LUMO + 2) are identical in **4a–c**$^{2+}$ and in **3**$^{2+}$. All four of these transitions (Figure 2) are clearly polarized along the short axis of thiapyrylogen in the *X*-direction. This is in stark contrast to the 355 and 401 nm low-energy bands in **TPP**$^{+}$, which have been assigned as two perpendicular chromophores, one polarized in the *X*- and the other in the *Y*-direction (*16*). The Y-band, which is a charge-transfer band from the 4-aryl ring to the pyrylium ring, is missing in **4a–c**$^{2+}$ and in **3**$^{2+}$ as a result of the electron-poor character of the 4-pyridinium ring.

All of the thiapyrylogens and **3**$^{2+}$ fluoresce and phosphoresce at the wavelengths depicted in Table 2. The singlet energies, S_1, were calculated from the crossing points of the normalized absorption and fluorescence emission spectra and the triplet energies, T_1, from the onset of the phosphorescence spectra (Table 2). The fluorescence quantum yields are smaller for pyrylogens than for **TPP**$^{+}$ and slightly smaller for thiapyrylogens than for pyrylogens (*e.g.* compare **4a**$^{2+}$ and **3**$^{2+}$). The weak fluorescent emission from **4a–c**$^{2+}$ and **3**$^{2+}$ is consistent with the previous suggestion that the Y-polarized chromophore, which is missing in pyrylogens, is the predominant fluorophore in pyrylium cations (*17*). Crude estimates of the relative phosphorescence quantum yields, Φ_P(rel), were obtained by comparing the absorbance-adjusted integrated phosphorescence

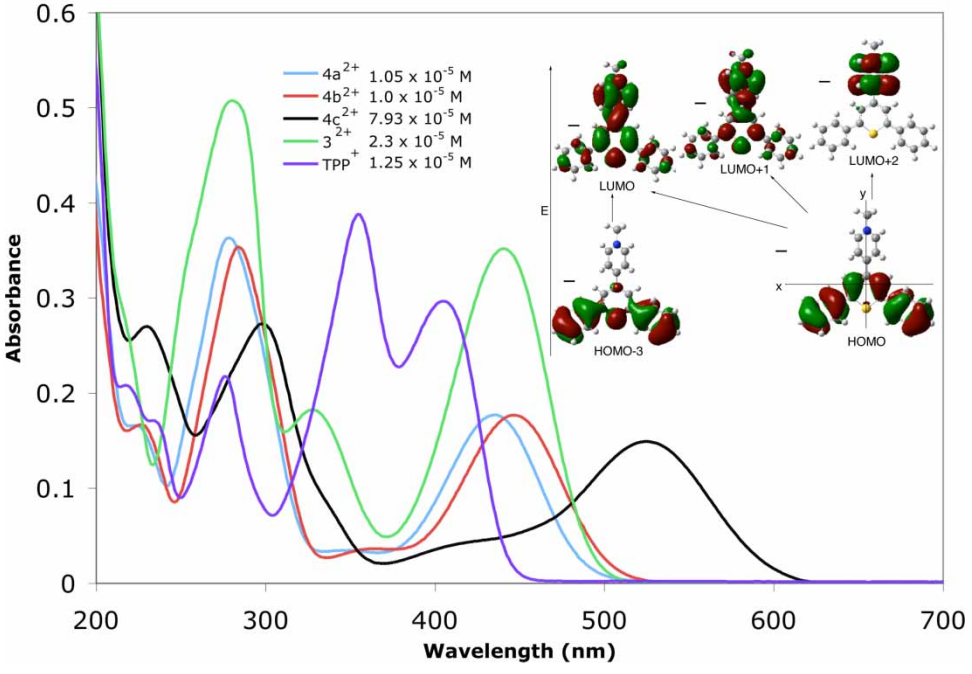

Figure 2. A comparison of the UV-visible spectra of **4a-c**$^{2+}$, **3**$^{2+}$, and 2,4,6-triphenylpyrylium tetrafluoroborate, **TPP**$^{+}$.

Table 2. Photophysical and electrochemical data for **4a–c**$^{2+}$, **3**$^{2+}$, and **TPP**$^{+}$.

	4a^{2+}	**4b**$^{2+}$	**4c**$^{2+}$	**3**$^{+}$	**TPP**$^{+}$
$E_{1/2}(1)^{\dagger}$	0.19	0.23	0.09	0.17	−0.35
$E_{1/2}(2)^{\dagger}$	−0.32	−0.28	−0.36	−0.35	−1.53
$\lambda_F^{\ddagger}$	547	571	662	533	465
$\lambda_P^{\S}$	581	580	662	565	520
$\tau_P^{\P}$	36.5 ± 0.5	29.6 ± 0.04	19.5 ± 0.2	35.6 ± 0.2	225 ± 3
$E(S_1)$	58	57	49	59	65[||]
$E(T_1)$	55	54	48	54	53[||]
Φ_F	0.13 ± 0.01	0.16 ± 0.03	f	0.18 ± 0.01	0.60[||]
Φ_P(rel)	1.00	0.74	0.28	0.17	0.92

Notes: f, Too weak to be measured accurately. [†]In volts versus SCE. [‡]In nanometers (nm) at 298 K. [§]In nm at 77 K in EtOH/HCl(g) glass. [¶]In milliseconds (ms) at 77 K in EtOH/HCl(g) glass. [||]From (*23*).

emissions. We speculate that the enhanced phosphorescence efficiencies in thiapyrylogens (Table 2) in comparison to their oxygen analogs are due to spin-orbit coupling-induced intersystem crossing and increased triplet formation.

Thiaprylogen **4a**$^{2+}$ was irradiated at 355 nm in CH_3CN containing 0.01% HBF_4 with 3 mJ/pulses from a Nd:YAG laser, and the transient absorption spectrum depicted in Figure 3 was collected. We assign the broad, fairly intense peak at ∼560 nm to the triplet based upon its sensitivity to quenching by oxygen. This transient species decays (inset in Figure 3) with a lifetime of 52 ± 3 μs, consistent with this assignment. Emission at 1270 nm in the near infrared from an oxygen saturated sample of **4a**$^{2+}$ was also detected at a 90° angle relative to the 355 nm laser flash. The lifetime of the emissive species increased upon doping the acetonitrile solution of **4a**$^{2+}$ with a deuterated solvent, consistent with its assignment as singlet oxygen ($^1\Delta_g$). In dramatic

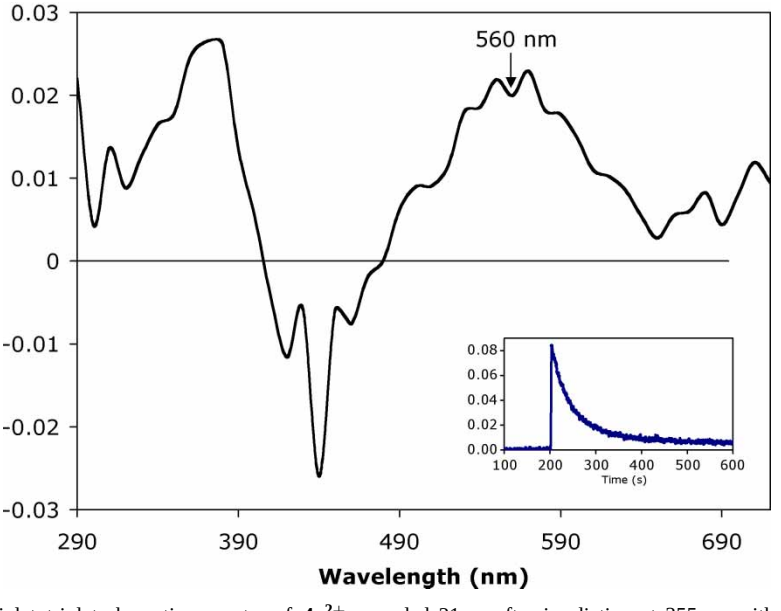

Figure 3. Triplet–triplet absorption spectra of **4a**$^{2+}$ recorded 21 μs after irradiation at 355 nm with a 3 mJ/pulse generated by a Nd:YAG laser. Inset: transient decay monitored at 560 nm.

contrast, the oxygen analogs of the thiapyrylogens do not sensitize formation of singlet oxygen (*9*). We attribute the ability of the thiapyrylogens to sensitize singlet oxygen formation to their enhanced intersystem crossing to the triplet manifold.

2.3. *Electrochemical and computational characterizations of 4a–c^{2+} and their redox partners*

The thiapyrylogens **4a–c**$^{2+}$ are reduced by cyclic voltammetry (CV) in two one-electron chemically reversible and electrochemically quasireversible steps at the potentials listed in Table 2. The chemical reversibility of the formation of the radical cations was unaffected by saturation of the CV samples with oxygen. In contrast, **TPP**$^{+}$ exhibits EC behavior, indicative of rapid reaction of **TPP**$^{\cdot}$ with oxygen (*18*). We attribute the lack of reactivity of the thiapyrylogen radical cations with oxygen, a characteristic they share with the 4,4′-pyrylogens (*9*), to the greater positive charge and greater spin delocalization in pyrylogens in comparison to **TPP**$^{\cdot}$. In addition, both the 4,4′-pyrylogen and the 4,4′-thiapyrylogen radical cations are thermodynamically incapable of reduction of oxygen to form superoxide ($E^0[O_2/O_2^-] = -0.87$ V versus SCE in CH_3CN) (*19*).

Replacement of the 4-phenyl ring in the thia analog (*20*) of **TPP**$^{+}$, **STPP**$^{+}$, with the pyridinium ring in **4a**$^{2+}$ increases the ease of the first reduction by 450 mV and the second reduction by over 920 mV (*20*). The effect on the first reduction potential is a result of the greater electron-withdrawing ability of a pyridinium in comparison to a phenyl ring. The even larger difference in the ease of the second reduction is also readily rationalized, since the addition of a second electron generates an anion with destabilizing electron–electron repulsion, **STPP**$^{-}$, in the case of **STPP**$^{+}$, but a closed shell neutral compound, **4a**°, in the case of **4a**$^{2+}$ (Scheme 3).

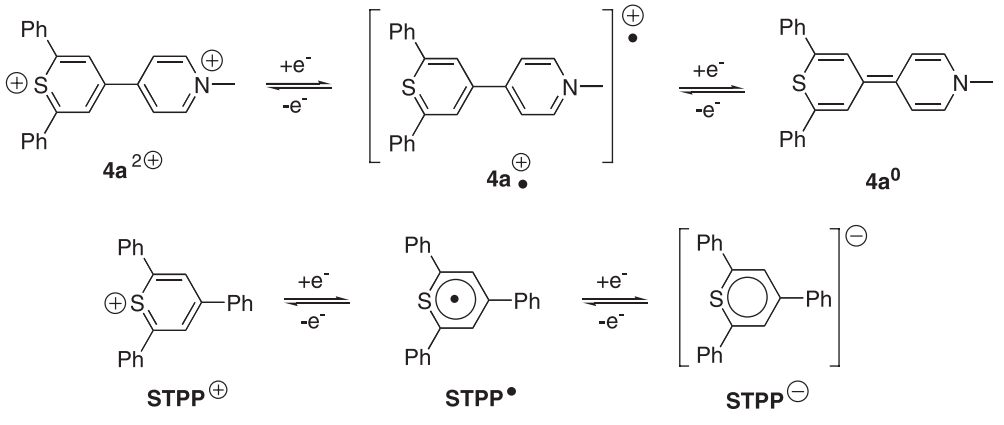

Scheme 3.

The B3LYP/6-31G(d) geometries of the products of the first reduction, the thiapyrylogen radical cations (Table 3), are very different from their dication precursors. The inter-ring bond distance, $d_{44'}$, is ∼0.05 Å shorter, and the inter-ring dihedral angle (>344′3′) is significantly smaller (*e.g.* **4a**$^{+\cdot}$[15.94°] → **4a**$^{2+}$[43.32°]) in the thiapyrylogen radical cation than in the dication. These geometry changes suggest an increase in the π-bond order of the inter-ring 4-4′ bond and a flattening of the thiapyrylogen core during reductions of the thiapyrylogen dications. The flattening of the pyrylogen core is more dramatic in pyrylogens than in thiapyrylogens, as revealed by a 12° smaller inter-ring dihedral angle (>344′3′) in **3**$^{+\cdot}$(3.53°) than in thiapyrylogen, **4a**$^{+\cdot}$(15.94°). In addition, the Mulliken spin densities are more evenly distributed in the pyridinium ring (0.46)

Table 3. B3LYP/6-31G(d) structural parameters for $\mathbf{3}^{+\cdot}$ and $\mathbf{4a–c}^{+\cdot}$.[†‡]

	$\mathbf{3}^{+\cdot}$	$\mathbf{4a}^{+\cdot}$	$\mathbf{4b}^{+\cdot}$	$\mathbf{4c}^{+}$[§]
d_{12} (Å)	1.365	1.755	1.757	1.759
d_{16} (Å)	1.365	1.755	1.757	1.759
$d_{44'}$ (Å)	1.435	1.442	1.442	1.441
$d_{1'2'}$ (Å)	1.370	1.368	1.367	1.369
$d_{1'6'}$ (Å)	1.369	1.368	1.367	1.370
d_{2a} (Å)	1.464	1.476	1.475	1.469
$d_{6a'}$ (Å)	1.464	1.476	1.475	1.469
>216	121.29°	103.38°	103.35°	103.73°
>2′1′6″	118.62°	118.64°	118.68°	118.57°
>344′3′	3.53°	15.94°	16.28°	16.37°
>12ab	21.71°	38.38°	37.68°	34.24°
>16a′b′	21.74°	38.35°	37.59°	34.66°
3′2′NCH$_3$	176.89°	176.79°	176.88°	176.60°

Notes: [†]ZPE corrected energies; $\mathbf{3}^{+\cdot}$ −1017.287146 Hartrees; $\mathbf{4a}^{+\cdot}$ −1340.254178 Hartrees; $\mathbf{4b}^{+\cdot}$ −2259.459149 Hartrees; $\mathbf{4c}^{+\cdot}$ −1569.241521 Hartrees. [‡]See structure $\mathbf{3}^{2+}$ for labeling. [§]ii-Isomer with methoxy methyl pointing in towards pyrylium oxygen.

and the pyrylium ring (0.48) of $\mathbf{3}^{+\cdot}$ than in the pyridinium ring (0.39) and the thiapyrylium ring (0.56) of $\mathbf{4a}^{+\cdot}$.

The UV-visible spectrum of the radical cation, $\mathbf{4a}^{+\cdot}$, was generated by treating an acetonitrile solution of $\mathbf{4a}^{2+}$ with zinc (Figure 4). The spectrum features a long wavelength band at 613 nm and higher energy bands at 412, 385, and 266 nm. The assignment to the radical cation was verified by TD-DFT calculations in CH_3CN using the polarization continuum model and the B3LYP/6-31G(d) geometry. The TD-DFT calculation predicts, in reasonable agreement with the experimental results, that the two lowest energy transitions appear at 617 nm (SOMO → SOMO + 2; $f = 0.0148$) and 599 nm (SOMO → SOMO = 1; $f = 0.3441$). Parenthetically, the observation of the radical cation at 613 nm provides confirmatory evidence that the transient

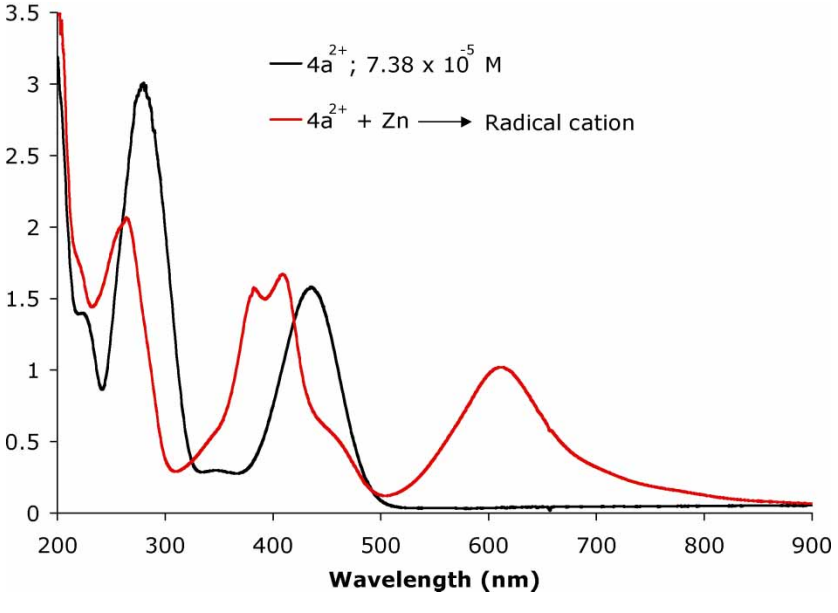

Figure 4. UV-visible spectra of $\mathbf{4a}^{2+}$ and its zinc reduction product.

Table 4. B3LYP/6-31G(d) structural parameters for $\mathbf{3^0}$ and $\mathbf{4a–c^0}$.[†‡]

	$\mathbf{3^0}$	$\mathbf{4a^0}$	$\mathbf{4b^0}$	$\mathbf{4c^{0\S}}$
d_{12} (Å)	1.386	1.787°	1.787°	1.787°
d_{16} (Å)	1.386	1.787°	1.788°	1.788°
$d_{44'}$ (Å)	1.390	1.398	1.399	1.398
$d_{1'2'}$ (Å)	1.387	1.384	1.383	1.385
$d_{1'6'}$ (Å)	1.387	1.384	1.383	1.385
d_{2a} (Å)	1.470	1.480	1.478	1.478
$d_{6a'}$ (Å)	1.470	1.479	1.478	1.478
>216	118.54°	101.46°	101.38°	101.60°
>2′1′6″	117.18°	117.14°	117.23°	117.09°
>344′3′	0.70°	1.8°	1.9°	2.50°
>12ab	19.07°	35.81°	34.99°	35.46°
>16a′b′	18.86°	36.00°	34.78°	35.76°
3′2′NCH$_3$	169.51°	171.17°	172.11°	170.50°

Notes: [†]ZPE corrected energies; $\mathbf{3}^{+\cdot}$ −1017.465607 Hartrees; $\mathbf{4a}^{+\cdot}$ −1340.435238 Hartrees; $\mathbf{4b}^{+\cdot}$ −2259.647629 Hartrees; $\mathbf{4c}^{+\cdot}$ −1569.415202 Hartrees. [‡]See structure $\mathbf{3}^{2+}$ for labeling. [§]ii-Isomer with methoxy methyl pointing in towards pyrylium oxygen.

species appearing at 560 nm in the laser flash photolysis studies (vide supra) is the triplet rather than the radical cation.

Conversion to the neutral thiapyrylogens **4a–c^0** leads to a further flattening of the thiapyrylogen core and nearly co-planar dispositions of the thiapyrylium and pyridinum rings. The inter-ring dihedral angle, <344′3′, is only 1.8°, 1.9°, and 2.5° in **4a^0**, **4b^0**, and **4c^0**, respectively (Table 4). In addition, the inter-ring bond distance, $d_{44'}$, is ∼0.04 Å shorter than in the radical cation and is consistent with an inter-ring double bond as depicted in Scheme 3 for **4a^0**.

3. Conclusion

The thiapyrylogens reported in this paper all have absorptions at wavelengths >430 nm, thereby allowing their use as sensitizers without concern about competitive absorption by most organic substrates. In addition, these thiapyrylogens can be used as singlet oxygen sensitizers or, since they are potent oxidants in their excited states, as electron transfer sensitizers. The S_1 states of **4a^{2+}**, **4b^{2+}**, and **4c^{2+}** are capable of oxidizing all organic substrates with oxidation potentials less than approximately 2.7, 2.7, and 2.2 eV, respectively. The T_1 states of **4a^{2+}**, **4b^{2+}**, and **4c^{2+}** are only slightly less oxidizing, with oxidation potentials of approximately 2.6, 2.6, and 2.2 eV, respectively.

4. Experimental

All the chemicals and solvents used for syntheses were reagent grade and used without further purification. Spectroscopic grade solvents were used for the UV-visible, fluorescence, phosphorescence, electrochemistry and the laser flash photolysis measurements. Melting points were determined using a Thomas Hoover UniMelt apparatus. The ^{1}H and ^{13}C NMR were recorded on a Bruker 400 MHz NMR spectrometer using TMS as the reference. UV-visible spectra were recorded on an Agilent 8453 spectrometer and emission measurements were done on a Cary Eclipse Fluorescence spectrometer. IR spectra of the compounds were recorded on a Nicolet NEXUS 470 FT-IR spectrometer. ESI-MS spectra were obtained on a Thermo-Finnigan LCQ

mass spectrometer. CV was conducted on CH Instruments CHI 600 potentiometer. Single-crystal X-ray diffraction was done using a Bruker P4-diffractometer.

4.1. *Synthesis of thiapyrylogens*

4.1.1. *4-(2,6-Di-phenyl thiapyrylium-4-yl)-1-methylpyridinium tetrafluoroborate* (**4a**$^{2+\bullet}$ **2BF$_4^-$**)

N-Methyl-1,5-diphenyl-3-(4-pyridyl)pentane-1,5-dione tetrafluoroborate (*9*) (430 mg, 1 mmol) was dissolved in 3 mL of acetic anhydride by heating to 45 °C. The solution was cooled back to room temperature and H_2S gas was purged through the solution for 1 h, while the solution turned to yellowish green in color. Boron trifluoride diethyletherate (600 μL, 4.8 mmol) was added using a syringe under a H_2S atmosphere. The mixture was heated to 70 °C initially under H_2S purging (10 min) and then without H_2S purging for 2 h. The reaction mixture was cooled to room temperature and 25 mL of diethyl ether was added. The solid formed was filtered and the yellowish product was recrystallized from acetic acid/acetonitrile mixture to yield yellow needle-shaped crystals (70%): m.p. 226–227 °C (decompose). IR (KBr) 1646, 1595 cm^{-1}. ESI-MS found 341.3; calcd 341.12. ^{1}H NMR (400 MHz, $CDCl_3$/trifluoroacetic acid [2:1]) δ 9.02 (s, 2H), 8.96 (d, $J = 6.6$ Hz, 2H), 8.61 (d, $J = 6.6$ Hz, 2H), 8.02 (d, $J = 8.0$ Hz, 4H), 7.86 (t, $J = 7.8$ Hz, 2H), 7.75 (t, $J = 7.8$ Hz, 4H), 4.55 (s, 3H). ^{13}C NMR (100 MHz, $CDCl_3$) δ 173.91, 155.62, 152.65, 146.74, 135.84, 133.37, 131.28, 131.26, 128.93, 128.23, 49.01.

4.1.2. *4-(2,6-Di-4-chlorophenyl thiapyrylium-4-yl)-1-methylpyridinium tetrafluoroborate* (**4b**$^{2+\bullet}$ **2BF$_4^-$**)

N-methyl-1,5-bis-(4-chlorophenyl)-3-(4-pyridyl)pentane-1,5-dione tetrafluoroborate (*9*) (488 mg, 1 mmol) was dissolved in 3 mL of acetic anhydride by heating to 45 °C. The solution was cooled back to room temperature and hydrogen sulfide gas was purged through the solution for 1 h. $BF_3{\bullet}Et_2O$ (600 μL, 4.8 mmol) was added, using a syringe, to the yellowish green solution, while the purging of the H_2S was continued. The mixture was heated to 70 °C initially under H_2S purging (10 min) and then without purging for 2 h. The reaction mixture was cooled to room temperature and diethyl ether (25 mL) was added to precipitate the yellow product, which was filtered and re-crystallized from an acetic acid acetonitrile mixture, yielding 430 mg (79%) of the product. m.p. 268–270 °C (decompose). IR (KBr) 1649, 1589 cm^{-1}. ESI-MS found 409.2; calcd 409.04. ^{1}H NMR (400 MHz, $CDCl_3$/trifluoroacetic acid [2:1]) δ 9.00 (s, 2H), 8.90 (d, $J = 6.7$ Hz, 2H), 8.55 (d, $J = 6.7$ Hz, 2H), 7.95 (d, $J = 8.7$ Hz, 4H), 7.70 (d, $J = 8.7$ Hz, 4H), 4.50 (s, 3H). ^{13}C NMR (100 MHz, $CDCl_3$) δ 172.55, 156.14, 152.86, 146.92, 144.01, 131.91, 131.74, 131.60, 130.25, 128.53, 49.19.

4.1.3. *4-(2,6-Di-4-methoxyphenyl thiapyrylium-4-yl)-1-methylpyridinium tetrafluoroborate* (**4c**$^{2+\bullet}$ **2BF$_4^-$**)

N-methyl-1,5-bis-(4-methoxyphenyl)-3-(4-pyridyl)pentane-1,5-dione tetrafluoroborate (*9*) (378 mg, 0.77 mmol) was dissolved in 3 mL of acetic anhydride by heating to 45 °C. Hydrogen sulfide gas was purged through the solution for 1 h. BF3·OEt (500 μL, 4.0 mmol) was added, using a syringe, to the solution, while the purging of H_2S was continued. The mixture was heated to 70 °C initially under H_2S purging (10 min) and then without purging for 2 h. The reaction mixture was cooled to room temperature and diethyl ether (25 mL) was added to precipitate the dark product, which was filtered and re-crystallized from an acetic acid acetonitrile mixture, yielding

302 mg (68%) of the product. m.p. 240–242 °C (decompose). IR (KBr) 1687, 1642, 1601 cm^{-1}. ESI-MS found 401.3; calcd 401.14. ^{1}H NMR (400 MHz, $CDCl_3$/trifluoroacetic acid [2:1]) δ 8.93 (d, $J = 6.8$ Hz, 2H), 8.71 (s, 2H), 8.55 (d, $J = 6.8$ Hz, 2H), 8.03 (d, $J = 9.0$ Hz, 4H), 7.22 (d, $J = 9.0$ Hz, 4H), 4.54 (s, 3H), 4.00 (s, 6H). ^{13}C NMR (100 MHz, $CDCl_3$) δ 170.61, 166.53, 154.18, 153.05, 146.55, 130.90, 127.89, 127.74, 126.03, 115.94, 56.23, 48.90.

4.1.4. *Zn dust reductions*

A 3 mL acetonitrile solution 7.38×10^{-5} M in $\mathbf{4a}^{2+}$ was placed into a side arm attached to a quartz cuvette. This solution was then subjected to three freeze-pump-thaw cycles and then tilted in order to pour the solution into the cuvette arm containing 38 mg (5.81×10^{-4} M) of zinc dust. The solution turned purple within 1 min and the color continued to intensify for 56 min and then ceased, signaling completion of the reaction. The UV-visible spectrum depicted in Figure 4 was then taken.

4.2. *Instrumental methods*

4.2.1. *Laser flash photolysis*

Triplet–triplet absorption spectra of $\mathbf{4a}^{2+}$ and $\mathbf{4b}^{2+}$ were collected using an excitation wavelength of 355 nm (5–20 mJ/pulse) from a Nd:YAG laser. The transient spectra were recorded with a point–point technique with 5–10 nm intervals from 350 to 700 nm. Samples were degassed by either three freeze-pump-thaw cycles or by bubbling with argon. The optical densities were adjusted to between 0.3 and 0.6 at the excitation wavelength. When oxygen was needed, the sample was saturated with oxygen for 20 min.

4.2.2. *Cyclic voltammetry*

The CV solutions were prepared containing 0.002 M substrate, 0.1 M $Bu_4N^+ClO_4^-$, and 0.002 M ferrocene in CH_3CN. All solutions were bubbled with argon for 20 min. The solutions were sealed tightly in a compartment with a glassy carbon electrode used as the working electrode, an $Ag/AgNO_3$ (0.01 M in MeCN) in MeCN reference electrode, and a platinum wire counter electrode.

4.2.3. *Crystallographic data for N-methyl-2,6-diphenyl-4,4′-thiapyrylogen* ($\mathbf{4a}^{2+}$)

[CCDC deposition number 714470] The X-ray diffraction data were measured at 150 K on a Bruker SMART APEX II CCD area detector system equipped with a graphite monochromator and an Mo Kα fine-focus sealed tube operated at 1.50 kW power (50 kV, 30 mA). A yellow rectangular prismatic crystal of approximate dimensions 0.44 mm × 0.24 mm × 0.11 mm was glued to a Hampton Research cryoloop using Paratone N oil. The detector was placed at a distance of 6.12 cm from the crystal during the data collection.

A series of narrow frames of data were collected with a scan width of 0.5° in ω or ϕ and an exposure time of 10 s per frame. The frames were integrated with the Bruker SAINT software package (*21*) using a narrow-frame integration algorithm. The integration of the data using a monoclinic unit cell yielded a total of 13,085 reflections in the 2θ range of 4.28–57.40°, of which 5127 were independent with $I \geq 2\sigma(I)$ ($R_{\text{int}} = 0.0237$). The data were corrected for absorption effects by the multi-scan method (SADABS). $\mathbf{4a}^{2+}\mathbf{(BF_4)_2}$ crystallizes in a chiral monoclinic space group, namely $P2_1$. The absolute structure was satisfactorily determined by refining the Flack

Parameter (*22*) to 0.02(6). Crystallographic data collection parameters and refinement data are collected in Table 1. The structure was solved by direct methods using the Bruker software package (*21*). The non-hydrogen atoms were located in successive Fourier maps and refined anisotropically. All hydrogen atoms were placed in calculated positions and refined isotropically by a riding model. The final refinement parameters are $R_1 = 0.0372$ and $wR_2 = 0.0991$ for data with $F > 4\sigma(F)$, giving the data to parameter ratio of 16. The refinement data for all data are $R_1 = 0.0397$ and $wR_2 = 0.1012$.

The asymmetric unit consists of a thiapyrylogen^{2+} cation and two tetrafluoroborate anions. The ions are well ordered and tightly packed, with the closest F$\cdots$H distances associated with the two borate anions and the thiapyrylogen cation being 2.587 Å (F4$\cdots$H17A) and 2.415 Å (F8$\cdots$H2A). The dication is non-planar as the thiapyrilium and pyridinium rings are twisted at 46.32(6)°. The two phenyl rings also deviate from the mean plane of the thiapyrilium ring, but the angles are comparatively smaller at 23.80(8)° and 26.43(9)°.

Acknowledgements

We thank the National Science Foundation for their generous support of this research.

Supporting Information

Computational details cyclic voltommetry, proton and carbon NMRs for 4a–c^{2+}, ESI-MS for 4a–c^{2+}.

References

(1) Rudorf, W.D. *Sci. Synth.* **2003,** *14*, 649–718.
(2) Niizuma, S.; Sato, N.; Kawata, H.; Suzuki, Y.; Toda, T.; Kokubun, H. *Bull. Chem. Soc. Jpn* **1985,** *58*, 2600–2607.
(3) Leonard, K.A.; Nelen, M.I.; Anderson, L.T.; Gibson, S.L.; Hilf, R.; Detty, M.R. *J. Med. Chem.* **1999,** *42*, 3942–3952.
(4) Leonard, K.A.; Nelen, M.I.; Simard, T.P.; Davies, S.R.; Gollnick, S.O.; Oseroff, A.R.; Gibson, S.L.; Hilf, R.; Chen, L.B.; Detty, M.R. *J. Med. Chem.* **1999,** *42*, 3953–3964.
(5) Parret, S.; Morlet-Savary, F.; Fouassier, J.P.; Inomata, K.; Matsumoto, T.; Heisel, F. *Bull. Chem. Soc. Jpn* **1995,** *68*, 2791–2795.
(6) Pettit, R. *Tetrahed. Lett.* **1960,** 11–13.
(7) Miranda, M.A. *Chem. Rev.* **1994,** *94*, 1063–1069.
(8) Wizinger, R.; Ulrich, P. *Helv. Chim. Acta* **1956,** *39*, 207–216.
(9) Clennan, E.L.; Liao, C.; Ayokosok, E. *J. Am. Chem. Soc.* **2008,** *130*, 7552–7553.
(10) Clennan, E. L., *Coord. Chem. Rev.* **2004,** *248*, 477–492.
(11) Gould, I. R.; Moser, J. E.; Armitage, B.; Farid, S.; Goodman, J. L.; Herman, M. S., *J. Am. Chem. Soc.* **1989,** *111*, 1917–1919.
(12) Morlet-Savary, F.; Parret, S.; Fouassier, J.P.; Inomata, K.; Matsumoto, T., *J. Chem. Soc. Faraday Trans.* **1998,** *94*, 745–752.
(13) Yoneda, S.; Sugimoto, T.; Yoshida, Z. *Tetrahedron* **1973,** *29*, 2009–2014.
(14) Frisch, M.J.; Trucks, G.W.; Schlegel, H.B.; Scuseria, G.E.; Robb, M.A.; Cheeseman, J.R.; Montgomery, Jr., J.A.; Vreven, T.; Kudin, K.N.; Burant, J.C.; Millam, J.M.; Iyengar, S.S.; Tomasi, J.; Barone, V.; Mennucci, B.; Cossi, M.; Scalmani, G.; Rega, N.; Petersson, G.A.; Nakatsuji, H.; Hada, M.; Ehara, M.; Toyota, K.; Fukuda, R.; Hasegawa, J.; Ishida, M.; Nakajima, T.; Honda, Y.; Kitao, O.; Nakai, H.; Klene, M.; Li, X.; Knox, J.E.; Hratchian, H.P.; Cross, J.B.; Bakken, V.; Adamo, C.; Jaramillo, J.; Gomperts, R.; Stratmann, R.E.; Yazyev, O.; Austin, A.J.; Cammi, R.; Pomelli, C.; Ochterski, J.W.; Ayala, P.Y.; Morokuma, K.; Voth, G.A.; Salvador, P.; Dannenberg, J.J.; Zakrzewski, V.G.; Dapprich, S.; Daniels, A.D.; Strain, M.C.; Farkas, O.; Malick, D.K.; Rabuck, A.D.; Raghavachari, K.; Foresman, J.B.; Ortiz, J.V.; Cui, Q.; Baboul, A.G.; Clifford, S.; Cioslowski, J.; Stefanov, B.B.; Liu, G.; Liashenko, A.; Piskorz, P.; Komaromi, I.; Martin, R.L.; Fox, D.J.; Keith, T.; Al-Laham, M.A.; Peng, C.Y.; Nanayakkara, A.; Challacombe, M.; Gill, P.M.W.; Johnson, B.; Chen, W.; Wong, M.W.; Gonzalez, C.; Pople, J.A. Gaussian 03, Revision C.02; Gaussian, Inc.: Wallingford, CT, 2004.
(15) Seminario, J.M., *Recent Developments and Applications of Modern Density Functional Theory*; Elsevier: New York, 1996.
(16) Balaban, A.T.; Fischer, G.W.; Dinculescu, A.; Koblik, A.V.; Dorofeendo, G.N.; Mezheritskii, V.V.; Schroth, W. *Pyrylium Salts: Synthesis, Reaction, and Physical Properties*; Academic Press: New York, 1982; Suppl. 2, p. 434.
(17) Montes-Navajas, P.; Teruel, L.; Corma, A.; Garcia, H. *Chem. Eur. J.* **2008,** *14*, 1762.

(18) Akaba, R.; Sakuragi, H.; Tokumaru, K. *J. Chem. Soc. Perkin Trans.* **1991,** *2*, 291–297.
(19) Sawyer, D.T., *Oxygen Chemistry*; Oxford University Press: New York, NY, 1991; p. 223.
(20) Akaba, R.; Kamata, M.; Koike, A.; Mogi, K.-I.; Kuriyama, Y.; Sakuragi, H. *J. Phys. Org. Chem.* **1997,** *10*, 861–869.
(21) APEX2 Software Suite V. 2.1-0, Bruker AXS: Madison, WI, 2004.
(22) Flack, H.D. *Acta Cryst. A* **1983,** *39*, 876–871.
(23) Miranda, M.A.; García, H. *Chem. Rev.* **1994**, *94*, 1063–1069.